IEEE Access
Multidisciplinary | Rapid Review | Open Access Journal

Received January 22, 2019, accepted March 21, 2019, date of publication March 29, 2019, date of current version July 10, 2019.

Digital Object Identifier 10.1109/ACCESS.2019.2908209

Synthetic Aperture Radar Interferometry Based on Vortex Electromagnetic Waves

XIANG-XI BU, ZHUO ZHANG, LONG-YONG CHEN, KE-HONG ZHU, SIYAN ZHOU, JIAN-PING LUO, RUICHANG CHENG, AND XING-DONG LIANG

National Key Lab of Microwave Imaging Technology, Institute of Electronics, Chinese Academy of Sciences, Beijing 100190, China
School of Electronics, Electrical and Communication Engineering, University of Chinese Academy of Sciences, Beijing 100049, China

Corresponding authors: Xiang-Xi Bu (buxiangxi14@mails.ucas.edu.cn) and Xing-Dong Liang (xdliang@mail.ie.ac.cn)

ABSTRACT The vortex electromagnetic (EM) wave carrying orbital angular momentum (OAM) offers a new degree of freedom for synthetic aperture radar (SAR) imaging. Because vortex EM waves have helical wavefronts, the vortex EM wave-based SAR echo contains the three-dimensional (3D) information of the target. In this paper, an OAM-based synthetic aperture radar interferometry (InSAR) technique is proposed to obtain 3D target information accurately without the existence of baseline. First, a vortex EM waves' SAR imaging model is established, and an improved range-Doppler algorithm is proposed correspondingly. Subsequently, the scheme of the OAM-based InSAR without the physical baseline is proposed. Compared with the conventional InSAR, the OAM-based InSAR can avoid the baseline decorrelation and reduce the requirement of the platform. Besides, the processing procedure of the OAM-based InSAR is simplified, which avoids the image registration and the interferogram flattening. The simulation results demonstrate the effectiveness of the proposed technique. Besides, the height estimation accuracy of the OAM-based InSAR was analyzed, in terms of interferometric phase error and OAM mode error. The height estimation accuracy can be improved by increasing the OAM mode difference appropriately. The OAM, which is completely independent of time, frequency, and polarization, offers a new scheme for the InSAR.

INDEX TERMS Vortex electromagnetic wave, orbital angular momentum, SAR, InSAR.

I. INTRODUCTION

Synthetic aperture radar interferometry (InSAR), which is a combination of Synthetic Aperture Radar (SAR) technique and interferometry technique, has been developed rapidly over several decades in Earth surface topography mapping and deformation detection [1]. The across-track InSAR, which is a standard configuration of InSAR, exploits the phase difference of at least two SAR images obtained from different positions to reveal the elevation information of the target area [2]. The distance between different positions is called baseline. However, the baseline is a paradox for InSAR. A large effective baseline, which is the basic precondition of high elevation estimation accuracy, always introduces the baseline decorrelation, which will deteriorate the interferometric phase seriously [3]. This tradeoff tremendously limits the performance of traditional across-track InSAR.

Orbital Angular Momentum (OAM) is an important physical quantity of electromagnetic (EM) waves, vortex EM waves with OAM have been widely studied in the past decade for communication [4] and radar applications [5]. The helical wavefront of vortex EM waves offers new potential solutions to radar imaging [6]. And recently, researches show that vortex EM waves of different OAM modes can be utilized in SAR imaging with great performance [7]. OAM presents to be a new degree of freedom (DOF) in SAR [8]–[10].

Without the existence of physical baseline, the OAM-based InSAR provides a novel approach for estimating the target three-dimensional (3D) information. In the proposed scheme, vortex EM waves of two different OAM modes are transmitted from one single OAM antenna, and the echoes are received by the same antenna. The obtained SAR images of different OAM modes have resolution elements with the same complex phase delay, but with a different OAM phase term. After interferometry, the common backscatter phase delay in each resolution element can be canceled, leaving a phase term proportional to the azimuth angle of the target, which can be used to derive the elevation information of the target. Compared with the traditional across-track InSAR, the OAM-based InSAR contains the following advantages: first, because only one single OAM antenna is used to

The associate editor coordinating the review of this manuscript and approving it for publication was Yang Li.

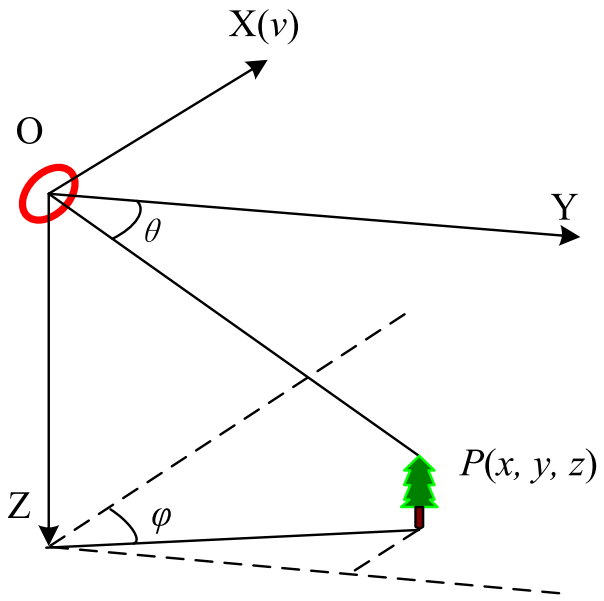

FIGURE 1. Geometry of the vortex EM waves based SAR imaging model.

transmit and receive the EM waves, the baseline no longer exists, which could reduce the requirement for InSAR platform and eliminate the effect of baseline decorrelation [3]. Moreover, because the propagation paths of two OAM beams are almost the same, the inhomogeneity effect of the propagation medium during the propagation path can be neglected. Last but not least, without the steps of image registration and interferogram flattening, the process of the OAM-based InSAR is simpler [2].

Due to the diversity of wavefronts, the OAM-based InSAR has the potential for mapping the Earth's surface topography accurately without the existence of baseline. To the best of our knowledge, there exist no public papers reporting the OAM-based InSAR technique. In this paper, a novel InSAR elevation estimation method based on vortex EM waves is proposed. The rest of this paper is composed of five parts. In Section II, the vortex EM waves based SAR imaging model is established, and the equations are derived in detail. In Section III, the improved Range-Doppler (R-D) algorithm is proposed, which solves the coupling problem between the azimuth time domain and the OAM domain. In Section IV, the OAM-based InSAR scheme is proposed, which is demonstrated by simulation results. In Section V, the elevation estimation accuracy is analyzed, in terms of the interferometric phase error and the OAM mode error. Finally, the conclusions are drawn in Section VI.

II. VORTEX EM WAVES SAR MODEL

The geometry of vortex EM waves based SAR imaging model is displayed in Fig. 1. The OAM antenna phase center (APC) is the origin of coordinate, and the platform is moving along the positive X-axis. The side-looking SAR operates in stripmap mode, which is preferred to guarantee a good spatial resolution and a wide swath width.

Let us assume that there is an ideal point target in the detection area. The coordinates of the target are $P(x, y, z)$ under the Cartesian coordinate or $P(r, \theta, \varphi)$ under polar coordinate. An N-element UCA antenna is used to transmit and receive vortex EM waves of the lth OAM mode [11]–[12]. Each element is multiplied by a different phase term, which transmits the linear frequency modulation (LFM) signal. The antenna look-down angle is 90 degree, which means that the transmitted OAM beam is propagating along the positive Y-axis. Considering the far field condition and supposing that N is large enough, the emitted signal $s_e(t_m, t, l)$ at $P(x, y, z)$ can be written as [7]:

$$\begin{aligned} s_e\left(t_m, t, l\right) \approx & N\omega_a\left(t_m - x/v\right)\omega_r\left(t - r\left(t_m\right)/c\right)\exp\left\{il\pi/2\right\} \\ & \times \exp\left\{i\pi K_r\left[t - r\left(t_m\right)/c\right]^2\right\}\exp\left\{il\varphi\left(t_m\right)\right\} \\ & \times \exp\left\{i2\pi f_c\left[t - r\left(t_m\right)/c\right]\right\} J_l\left[ka\sin\theta(t_m)\right] \end{aligned} \tag{1}$$

where t is the range time; t_m is the azimuth time; $\omega_r(t)$ is the range envelope; $\omega_a(t_m)$ is the azimuth envelope; K_r is the LFM ratio; f_c is the central frequency of the signal; c is the speed of light; a is the radius of the UCA antenna; $J_l\left[ka\sin\theta(t_m)\right]$ denotes the lth order Bessel function of the first kind; $r(t_m)$ is the slant range; $\theta(t_m)$ is the polar angle; and $\varphi(t_m)$ is the azimuth angle.

Combining the geometry relevance among the two coordinates, we can obtain the spherical coordinate of the target $P(r(t_m), \theta(t_m), \varphi(t_m))$ [7]:

$$r(t_m) = \sqrt{(x - vt_m)^2 + y^2 + z^2} \approx R_0 + \frac{v^2}{2R_0}\left(t_m - \frac{x}{v}\right)^2, \tag{2}$$

$$\theta(t_m) = \sin^{-1}\left\{\frac{\sqrt{(x - vt_m)^2 + z^2}}{\sqrt{R_0^2 + (x - vt_m)^2}}\right\} \tag{3}$$

where v is the flight speed;

$$R_0^2 = y^2 + z^2 \tag{4}$$

where R_0 is the shortest slant range between the APC and $P\left(x, y, z\right)$. After the Taylor series expansion of the instantaneous azimuth angle, which is resulted in:

$$\varphi(t_m) = \tan^{-1}\left\{\frac{y}{x - vt_m}\right\} \approx \varphi - \frac{vt_m}{z}, \tag{5}$$

$$\varphi = \arctan(\frac{y}{x}) \approx \frac{\pi}{2} + \frac{x}{z} \tag{6}$$

where φ is the initial azimuth angle of the target. After summing up all the signals received by the elements, the received signal $s_r\left(t_m, t, l\right)$ can be expressed as:

$$\begin{aligned} s_r\left(t_m, t, l\right) \approx & \sigma N^2\omega_a\left(t_m - x/v\right)\omega_r\left(t - 2r\left(t_m\right)/c\right)\exp\left\{il\pi\right\} \\ & \times \exp\left\{i\pi K_r\left[t - 2r\left(t_m\right)/c\right]^2\right\} J_l^2\left[ka\sin\theta(t_m)\right] \\ & \times \exp\{i2\pi f_c[t - 2r(t_m)/c]\}\exp\{i2l(\varphi - vt_m/z)\} \end{aligned} \tag{7}$$

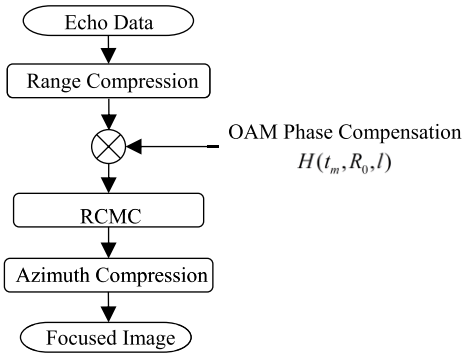

FIGURE 2. Flowchart of the improved Range-Doppler (*R-D*) algorithm.

where σ denotes the constant radar cross section (RCS) of the target.

It can be observed from (7) that, the phase terms of the received signal are similar to that of the traditional SAR echo except for the OAM phase term. Due to the added OAM phase term, the azimuth time domain is coupled with the OAM domain, which means that the target position in Doppler domain will change among different OAM modes. Thus, the azimuth defocus will appear if we use the traditional imaging processing algorithm, e.g., *R-D* algorithm [13].

III. PROCESSING ALGORITHM

In this section, an improved *R-D* algorithm for vortex EM waves SAR imaging is proposed, which can solve the coupling problem between the azimuth time domain and the OAM domain. The flowchart of the proposed algorithm is shown in Fig. 2.

After range compression of (7), the derived signal can be expressed as:

$$\begin{aligned} s_r(t_m, t, l) \approx \sigma N^2 \exp\{il\pi\} J_l^2 [ka \sin\theta(t_m)] \, p_r\left(t - \frac{2r(t_m)}{c}\right) \\ \times \omega_a\left(t_m - \frac{x}{v}\right) \exp\{i2l\varphi_0\} \exp\left\{-i2l\frac{vt_m}{z}\right\} \\ \times \exp\left\{-i\frac{4\pi R_0}{\lambda}\right\} \exp\left\{-i\pi K_a\left(t_m - \frac{x}{v}\right)^2\right\} \quad (8) \end{aligned}$$

where p_r is the range compressed pulse envelope; $K_a = 2v^2/\lambda R_0$ is the azimuth frequency modulation ratio.

In (8), the coupled OAM phase term, which varies with the azimuth slow time, will affect the range cell migration correction (RCMC) and the azimuth compression result. To compensate the coupled OAM phase term, the Z-axis component of the target is approximate to $R_0 \cos\beta_c$ where β_c is the incidence angle of the scene center. Therefore, in two-dimensional (2D) time domain, the $H(l, t_m, R_0)$ can be used to compensate the OAM phase terms before azimuth compression:

$$H(l, t_m, R_0) = \exp\left(i2l\frac{vt_m}{R_0 \cos\beta_c}\right) \exp\{-il\pi\}. \quad (9)$$

TABLE 1. Simulation parameters.

Carrier Frequency (f_c)	15 GHz
PRF	2000 Hz
Bandwidth (Δf_r)	150 MHz
Sampling Frequency	250 MHz
Platform Speed (v)	50 m/s
OAM Mode	+1

Finally, after RCMC and azimuth compression, the point spread function (PSF) of the target is expressed as:

$$\begin{aligned} s(t_m, t, l) = \sigma N^2 J_l^2 [ka \sin\theta(t_m)] \operatorname{sinc}[\Delta f_r (t - 2R_0/c)] \\ \times \operatorname{sinc}[\Delta f_a (t_m - x/v)] \exp\{i2l\varphi\} \quad (10) \end{aligned}$$

where Δf_r is the transmitted signal bandwidth and Δf_a is the Doppler bandwidth.

The azimuth resolution ρ_a is decided by the effective azimuth beam width θ_{BW}, and ρ_a can be expressed as [14]:

$$\rho_a = \lambda / 2\theta_{BW} \quad (11)$$

where $\lambda = c/f_c$ is the wavelength.

The range information is obtained by the pulse compression technique, and range resolution ρ_r can be expressed as [14]:

$$\rho_r = c/2\Delta f_r. \quad (12)$$

Simulations are carried out to demonstrate the effectiveness of the proposed algorithm. The imaging geometry is displayed in Fig. 1, and the UCA antenna is used to generate the desired OAM beams. Three ideal point targets in different azimuth positions are simulated, and their locations (x, R_0) are set as $P1$ (−2, 1000), $P2$ (0, 1000), $P3$ (2, 1000), respectively. Other simulation parameters are listed in Table 1. First of all, range compression of the echo signal is conducted. Subsequently, the coupled OAM phase term is compensated in the 2D time domain using the incidence angle of scene center P2. Finally, the vortex EM waves SAR image can be obtained after RCMC and azimuth compression, which is shown in Fig. 3. The results indicate that targets can be focused well using the proposed algorithm.

For target P3 that is not located in the scene center, the azimuth profile comparison between the improved *R-D* algorithm and the conventional *R-D* algorithm is shown in Fig. 4. Table 2 shows the evaluation performance of P3 in Fig. 4. It can also be seen from Fig. 4 and Table 2 that the side lobe rises and the main lobe deviates if we use the conventional *R-D* algorithm, which will seriously deteriorate the imaging quality. The simulation results validate the effectiveness of the improved *R-D* algorithm.

IV. OAM-BASED InSAR

InSAR employs two complex-valued SAR images to derive the target information using the phases of two images [15].

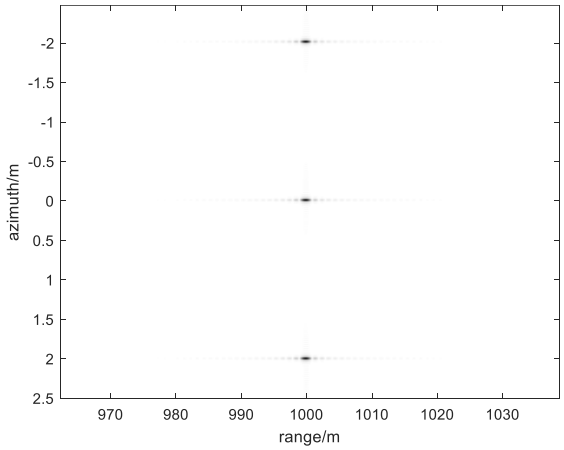

FIGURE 3. Vortex EM waves SAR imaging result using the improved *R-D* algorithm.

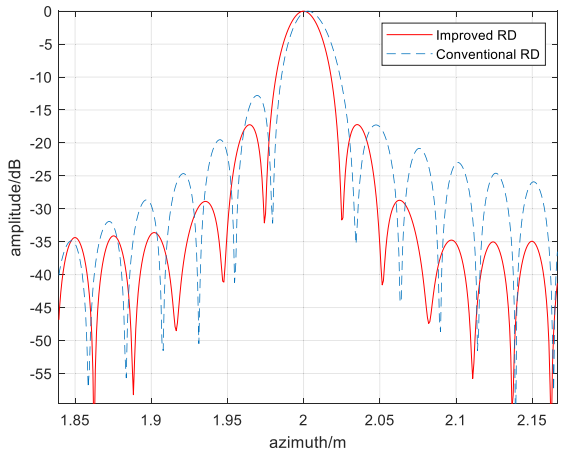

FIGURE 4. Azimuth profile comparison of *P*3. The red solid line denotes the result of the improved *R-D* algorithm with orbital angular momentum (OAM) phase term compensation, while the blue dashed line denotes the result of conventional *R-D* algorithm without OAM phase term compensation.

TABLE 2. Evaluation of azimuth profile in Fig. 4.

Azimuth Profile	Resolution (m)	PSLR (dB)	ISLR (dB)
Solid line	0.03	−17.21	−15.34
Dashed line	0.03	−12.79	−11.86

The difference between the two images depends on at least one parameter, e.g., flight path, acquisition time, wavelength, and so on [16]. Generalizing this concept, the OAM-based InSAR is a novel scheme of InSAR to obtain the 3D information of the target, where the different parameter is the OAM mode number.

The OAM-based InSAR requires only one OAM antenna, e.g., the UCA antenna, which could transmit and receive two different OAM modes in a ping-pong fashion. After 2D imaging process using the improved *R-D* algorithm separately, the images of two OAM modes can be expressed as referring to equation (10):

$$s_1(t_m, t, l_1) = \sigma N^2 J_{l_1}^2 [ka \sin\theta(t_m)] \operatorname{sinc}[\Delta f_r (t - 2R_0/c)] \times \operatorname{sinc}[\Delta f_a (t_m - x/v)] \exp\{i2l_1\varphi\}, \quad (13)$$

$$s_2(t_m, t, l_2) = \sigma N^2 J_{l_2}^2 [ka \sin\theta(t_m)] \operatorname{sinc}[\Delta f_r (t - 2R_0/c)] \times \operatorname{sinc}[\Delta f_a (t_m - x/v)] \exp\{i2l_2\varphi\}. \quad (14)$$

Then, multiply the image s_1 by the conjugated image s_2, and subsequently, the interferogram can be expressed as:

$$v = s_1 s_2^* = |s_1||s_2| \exp\{i\Delta\phi\}, \quad (15)$$

$$\Delta\phi = 2\Delta l\varphi \quad (16)$$

where Δl is the OAM mode difference, and $\Delta\phi$ is the interferometric phase, which is proportional to the initial azimuth angle of the target. Since the interferometric phase is obtained from an argument computation, which will be ambiguous within integer multiples of 2π, especially when Δl is large, i.e.,

$$\Delta\phi = \psi + 2k\pi \quad (17)$$

where ψ denotes the principle value of the phase, or the wrapped phase. To recover the true value of the interferometric phase, the phase unwrapping is needed. Some reference points with known initial azimuth angles can be used for phase unwrapping to derive the integral number k in (17). In the future, we will carry out more theoretical work on the phase unwrapping problem in the OAM-based interferometry.

After phase unwrapping, the following equations are used to deduce the height h of the target.

$$h = H - z, \quad (18)$$

$$z = \sqrt{R_0^2 - y^2}, \quad (19)$$

$$y = x \tan\varphi, \quad (20)$$

$$\varphi = \frac{\Delta\phi}{2\Delta l}. \quad (21)$$

According to (18), (19), (20), and (21), the height h of the target can be expressed as:

$$h = H - \sqrt{R_0^2 - (x \tan\frac{\Delta\phi}{2\Delta l})^2} \quad (22)$$

where H denotes the flight height, which can be measured accurately, and the azimuth position x and the shortest slant range R_0 can be derived from the 2D SAR imaging results [17].

As shown in Fig. 5, the process of the OAM-based InSAR contains the following steps:

1). Imaging processing using the improved *R-D* algorithm to get the 2D SAR images of two OAM modes separately;

2). Multiplying two images to obtain the interferogram;

3). Phase unwrapping;

4). 3D reconstruction of the target.

Since vortex EM waves of two different OAM modes are transmitted and received by the same antenna, the data processing procedure of our proposed scheme is

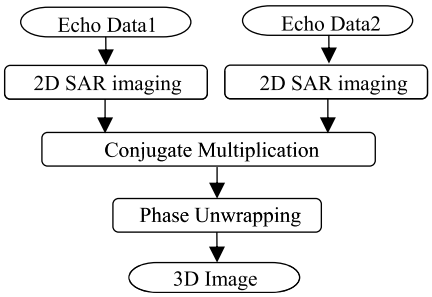

FIGURE 5. Flowchart of the OAM-based InSAR process.

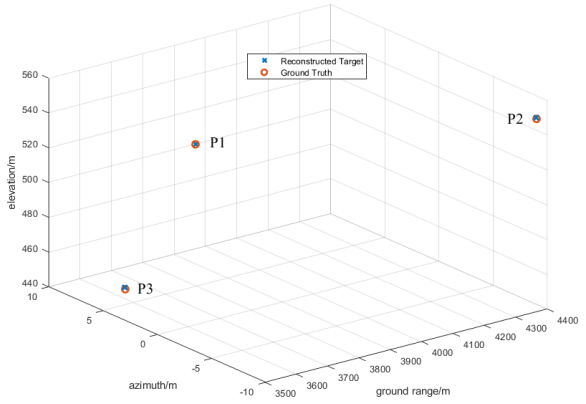

FIGURE 6. 3D imaging result using OAM-based interferometry. The red dot denotes the ground truth, while the blue x denotes the reconstructed target.

simpler compared with the conventional InSAR process, e.g., the image registration and the interferogram flattening can be avoided [2].

In order to verify the effectiveness of the height estimation method using the OAM-based InSAR, a proof-of-concept simulation was carried out. In the simulation, three ideal point targets are placed in the scene, and the positions are set as P1 (10, 3969, 500), P2 (5, 4365, 551), P3 (−10, 3572, 448), respectively under Cartesian coordinate system. Vortex EM waves of OAM mode +1 and −1 are used for interferometry. The SNR is set as 30 dB, and other simulation parameters are the same as those in Table 1.

Firstly, the 2D SAR images of two modes are derived using the improved *R-D* algorithm as described before. Secondly, multiplying the image of mode +1 by the conjugated image of mode −1 to obtain the interferometric phase. After phase unwrapping, the 3D information can be derived according to (19-21). The 3D reconstructed result is shown in Fig. 6. The positions of the reconstructed targets are located at P1 (10, 3969.1, 499.9), P2 (5, 4364.8, 551.7), P3 (−10, 3571.8, 448.2), respectively. It can be observed that the 3D position of the target can be reconstructed accurately. Because in the improved *R-D* algorithm, the incidence angle of the scene center is used for OAM phase compensation, the target P1 which has the same incidence angle can be reconstructed with high precision. Whereas for other target, such as P2 or P3 with different incidence angle, the reconstruction accuracy decreases. The simulation results validate the effectiveness of the height estimation method using the OAM-based InSAR technique.

V. HEIGHT ESTIMATION ACCURACY

According to (22), the height estimation accuracy is determined by the errors of the flight height, the slant range, the azimuth position, the interferometric phase, and the OAM mode difference. Differentiating (22) with respect to each individual parameter, we can derive that:

$$\delta h_H = \sigma_H, \tag{23}$$

$$\delta h_x = \frac{x\left(\tan\frac{\Delta\phi}{2\Delta l}\right)^2}{\sqrt{R_0^2-(x\tan\frac{\Delta\phi}{2\Delta l})^2}}\sigma_x, \tag{24}$$

$$\delta h_{R_0} = -\frac{R_0}{\sqrt{R_0^2-(x\tan\frac{\Delta\phi}{2\Delta l})^2}}\sigma_{R_0}, \tag{25}$$

$$\delta h_{\Delta l} = -\frac{x^2\Delta\phi\tan\frac{\Delta\phi}{2\Delta l}}{2\Delta l^2(\cos\frac{\Delta\phi}{2\Delta l})^2\sqrt{R_0^2-(x\tan\frac{\Delta\phi}{2\Delta l})^2}}\sigma_{\Delta l}, \tag{26}$$

$$\delta h_{\Delta\phi} = \frac{x^2\tan\frac{\Delta\phi}{2\Delta l}}{2\Delta l(\cos\frac{\Delta\phi}{2\Delta l})^2\sqrt{R_0^2-(x\tan\frac{\Delta\phi}{2\Delta l})^2}}\sigma_{\Delta\phi} \tag{27}$$

where σ_H denotes the root-mean-square error (RMSE) of flight height; σ_{R_0} denotes the RMSE of slant range; σ_x denotes the RMSE of azimuth position; $\sigma_{\Delta\phi}$ denotes the RMSE of interferometric phase; $\sigma_{\Delta l}$ denotes the RMSE of OAM mode difference.

Assuming that the above parameters are independent error contributors, we can evaluate the height estimation accuracy according to:

$$\begin{aligned}\sigma_h^2 = {} & \frac{x^2\left(\tan\frac{\Delta\phi}{2\Delta l}\right)^4}{R_0^2-(x\tan\frac{\Delta\phi}{2\Delta l})^2}\sigma_x^2+\frac{R_0^2}{R_0^2-(x\tan\frac{\Delta\phi}{2\Delta l})^2}\sigma_{R_0}^2 \\ & +\sigma_H^2+\frac{x^4\Delta\phi^2(\tan\frac{\Delta\phi}{2\Delta l})^2}{4\Delta l^4(\cos\frac{\Delta\phi}{2\Delta l})^4(R_0^2-(x\tan\frac{\Delta\phi}{2\Delta l})^2)}\sigma_{\Delta l}^2 \\ & +\frac{x^4(\tan\frac{\Delta\phi}{2\Delta l})^2}{4\Delta l^2(\cos\frac{\Delta\phi}{2\Delta l})^4(R_0^2-(x\tan\frac{\Delta\phi}{2\Delta l})^2)}\sigma_{\Delta\phi}^2\end{aligned} \tag{28}$$

where σ_h denotes the RMSE of the target height.

The measurement error of the flight height is relatively small, which is not a critical contributor to height estimation. Equation (24), and (25) show that the height errors arise from the uncertainties of the azimuth position and the slant range, which correspond to the system parameters, as well as the imaging algorithm [18].

The mode characteristics of vortex EM waves, e.g. the OAM mode purity, will cause uncertainties on the OAM mode difference, which will finally translate into height

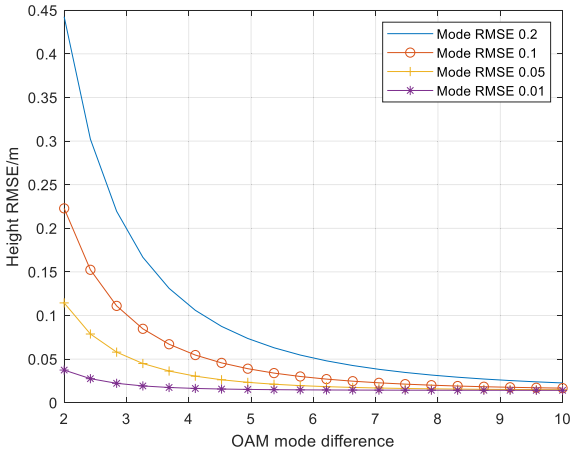

FIGURE 7. Height estimation error versus OAM mode difference under different OAM mode errors.

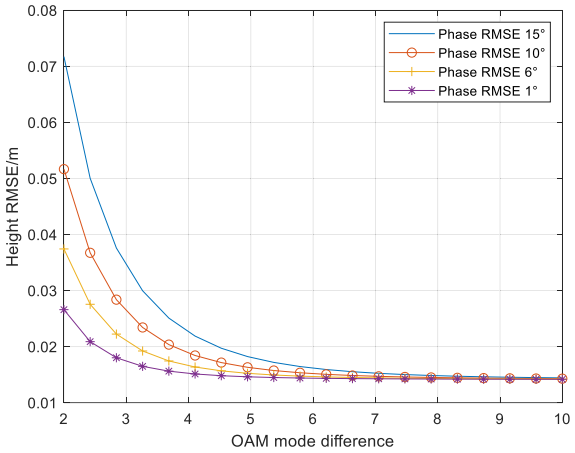

FIGURE 8. Height estimation error versus OAM mode difference under different interferometric phase errors.

TABLE 3. Simulation parameters.

Carrier Frequency (f_c)	15 GHz
Slant range RMSE	0.01 m
Azimuth position RMSE	0.01 m
Flight Height RMSE	0.01 m
Interferometric phase RMSE	6°

estimation errors in topographic applications, as displayed in (26). Fig. 7 shows the height estimation error versus OAM mode difference under different OAM mode errors, and the simulation parameters are listed in Table 3. The simulation result indicates that the height estimation accuracy can be improved by decreasing the OAM mode difference error.

In our scheme, the UCA antenna is used to generate the vortex EM waves, and the mode purity is determined by four factors: the number of elements N, the OAM mode number l, the array radius a, and the elevation angle θ [19]. Vortex EM waves with pure mode can be obtained by optimizing the UCA antenna properly, such as increasing the element number, and decreasing the array radius. Besides, the actual mode is a mixture of a series of discrete modes with periodicity of the element number N, where the fundamental mode is the maximum mode. In some appropriate elevation angles, the radiation fields are located in the pure mode region, which has little influence on the practical applications [19].

The height estimation error with respect to the interferometric phase error is presented in Fig. 8. The RMSE of the OAM mode difference error is 0.01, and other simulation parameters are the same as those in Table 3. Signal-to-noise ratios (SNR), the extra OAM phase error introduced by the processing algorithm, and the inherent system errors are main contributors to the interferometric phase errors. The simulation result indicates that the height estimation accuracy can be improved by decreasing the interferometric phase error.

Besides, it can be observed from both Fig. 7 and Fig. 8 that the height estimation accuracy improves with the increase of OAM mode difference. When the OAM mode difference increases to a certain extent, the improvement is relatively limited. Thus, an appropriate OAM mode difference is preferred to guarantee the height estimation accuracy, as well as the system complexity.

In the OAM-based interferometry, since the two OAM beams are transmitted and received by the same antenna, the physical baseline no longer exists, which can reduce the flight platform complexity, and avoid the baseline decorrelation. Because the propagation paths of two OAM beams are almost the same,, the inhomogeneity effect of the propagation medium during the propagation path can be neglected, and moreover the temporal decorrelation has little effect on the interferometry process. It should be noted that the OAM-based InSAR cannot reconstruct the targets in the zero-Doppler plane, i.e., their initial azimuth angles are $\pi/2$.

VI. CONCLUSION

This paper has given a comprehensive study of the OAM-based InSAR. The vortex EM waves based SAR imaging model was built and the corresponding imaging algorithm was proposed. Simulation results demonstrate the effectiveness of the proposed algorithm.

The OAM-based InSAR technique is proposed to reconstruct the 3D target information accurately without the existence of physical baseline. Compared with conventional InSAR, the OAM-based InSAR could eliminate the baseline decorrelation and reduce the requirement for the platform. Simulation results demonstrate the effectiveness of the proposed technique. Besides, the height estimation accuracy of the OAM-based InSAR was analyzed, in terms of interferometric phase error and OAM mode error, etc. The accuracy can be improved by increasing the OAM mode difference appropriately.

Furthermore, the OAM-based InSAR can also be combined with other baselines, e.g., the spatial baseline and the

temporal baseline, to obtain more information of the target. This work shows the new application of vortex EM waves, which advances the development of novel InSAR systems. Our future work will include a proof-of-concept experiment of the OAM-based InSAR technique.

ACKNOWLEDGMENT

The authors would like to thank the anonymous reviewers for their valuable comments and suggestions.

REFERENCES

[1] R. Bamler and P. Hartl, "Synthetic aperture radar interferometry," *Inverse Problems*, vol. 14, no. 4, p. R1, 1998.
[2] S. N. Madsen and H. A. Zebker, "Synthetic aperture radar interferometry: Principles and applications," in *Manual of Remote Sensing*, vol. 3. Boston, MA, USA: Artech House, 1999, ch. 6.
[3] E. Rodríguez and J. M. Martin, "Theory and design of interferometric synthetic-aperture radars," *Proc. IEEE*, vol. 139, no. 2, pp. 147–159, Apr. 1992.
[4] F. Tamburini, E. Mari, A. Sponselli, B. Thidé, A. Bianchini, and F. Romanato, "Encoding many channels on the same frequency through radio vorticity: First experimental test," *J. Phys.*, vol. 14, no. 3, pp. 811–815, Mar. 2012.
[5] K. Liu, Y. Cheng, Z. Yang, H. Wang, Y. Qin, and X. Li, "Orbital-angular-momentum-based electromagnetic vortex imaging," *IEEE Antennas Wireless Propag. Lett.*, vol. 14, pp. 711–714, 2015.
[6] K. Liu, Y. Cheng, Y. Gao, X. Li, Y. Qin, and H. Wang, "Super-resolution radar imaging based on experimental OAM beams," *Appl. Phys. Lett.*, vol. 110, no. 16, Apr. 2017, Art. no. 164102.
[7] X. Bu, Z. Zhang, L. Chen, X. Liang, H. Tang, and X. Wang, "Implementation of vortex electromagnetic waves high-resolution synthetic aperture radar imaging," *IEEE Antennas Wireless Propag. Lett.*, vol. 17, no. 5, pp. 764–767, May 2018.
[8] T. Yang, S. Li, O. Xu, W. Li, and Y. Wang, "Three dimensional SAR imaging based on vortex electromagnetic waves," *Remote Sens. Lett.*, vol. 9, no. 4, pp. 343–352, 2018.
[9] X. Bu, Z. Zhang, X. Liang, L. Chen, H. Tang, Z. Zeng, and J. Wang, "A novel scheme for MIMO-SAR systems using rotational orbital angular momentum," *Sensors*, vol. 18, no. 10, p. 3511, 2018.
[10] J. Wang, K. Liu, Y. Cheng, and H. Wang, "Three-dimensional target imaging based on vortex stripmap SAR," *IEEE Sensors J.*, vol. 19, no. 4, pp. 1338–1345, Feb. 2019.
[11] B. Thidé, H. Then, J. Sjöholm, K. Palmer, J. Bergman, T. D. Carozzi, Y. N. Istomin, N. H. Ibragimov, and R. Khamitova, "Utilization of photon orbital angular momentum in the low-frequency radio domain," *Phys. Rev. Lett.*, vol. 99, no. 8, Aug. 2007, Art. no. 087701.
[12] S. M. Mohammadi, L. K. S. Daldorff, J. E. S. Bergman, R. L. Karlsson, B. Thide, K. Forozesh, T. D. Carozzi, and B. Isham, "Orbital angular momentum in radio—A system study," *IEEE Trans. Antennas Propag.*, vol. 58, no. 2, pp. 565–572, Feb. 2010.
[13] I. G. Cumming, and F. H. Wong, *Digital Processing of Synthetic Aperture Radar Data: Algorithms and Implementation*. Norwood, MA, USA: Artech House, 2005.
[14] J. Kovaly, *Synthetic Aperture Radar*. Boston, MA, USA: Artech House, 1976.
[15] L. C. Graham, "Synthetic interferometer radar for topographic mapping," *Proc. IEEE*, vol. 62, no. 6, pp. 763–768, Jun. 1974.
[16] R. Gens and J. L. Van Genderen, "SAR interferometry-Issues, techniques, applications," *Int. J. Remote Sens.*, vol. 17, no. 10, pp. 1803–1835, 1996.
[17] J. C. Curlander and R. N. McDonough, *Synthetic Aperture Radar: Systems and Signal Processing*. New York, NY, USA: Wiley, 1991.
[18] F. K. Li and R. M. Goldstein, "Studies of multibaseline spaceborne interferometric synthetic aperture radars," *IEEE Trans. Geosci. Remote Sens.*, vol. 28, no. 1, pp. 88–97, Jan. 1990.
[19] T. Yuan, Y. Cheng, H. Wang, and Y. Qin, "Mode characteristics of vortical radio wave generated by circular phased array: Theoretical and experimental results," *IEEE Trans. Antennas Propag.*, vol. 65, no. 2, pp. 688–695, Feb. 2017.

XIANG-XI BU was born in Jinan, China, in 1991. He received the B.Sc. degree in electronic information science and technology from Jilin University, Changchun, China, in 2014. He is currently pursuing the Ph.D. degree in signal and information processing with the National Key Lab of Microwave Imaging Technology, Institute of Electronics, Chinese Academy of Sciences.

His research interests include the application of vortex electromagnetic wave, radar system design, and novel radar imaging techniques.

ZHUO ZHANG received the B.Sc. and Ph.D. degrees from the Beijing Institute of Technology, Beijing, China, in 2007 and 2012, respectively.

Since 2012, he has been with the National Key Lab of Microwave Imaging Technology, Institute of Electronics, Chinese Academy of Sciences. During this period, he has product responsibility for antenna systems, synthetic aperture radar systems, and passive radar systems. He is currently an Associate Professor with the National Key Lab of Microwave Imaging Technology. His research interests include array antennas, antenna measurement, and novel radar imaging techniques.

LONG-YONG CHEN received the B.Sc. degree in electrical engineering from the University of Science and Technology of China, Anhui, China, in 2003, and the M.Sc. and Ph.D. degrees in signal and information processing from the University of Chinese Academy of Sciences, Beijing, China, in 2006 and 2009, respectively.

Since 2009, he has been with the National Key Lab of Microwave Imaging Technology, Institute of Electronics, Chinese Academy of Sciences. During this period, he has product responsibility for millimeter-wave radars, receivers, polarimetric and interferometric synthetic aperture radar (SAR) systems, and multiple-input–multiple-output SAR systems. He is currently a Professor with the National Key Lab of Microwave Imaging Technology. His research interests include radar signal processing, coherent polarimetric and interferometric SAR system designing, and novel radar imaging techniques.

KE-HONG ZHU was born in Chongqing, China, in 1992. He received the B.Sc. degree in communication engineering from the Beijing Institute of Technology, Beijing, China, in 2014. He is currently pursuing the Ph.D. degree in signal and information processing with the National Key Lab of Microwave Imaging Technology, Institute of Electronics, Chinese Academy of Sciences.

His research interests include radar waveform designing and processing, and novel radar imaging techniques.

SIYAN ZHOU was born in Chongqing, China, in 1995. She received the B.Sc. degree in electronic information engineering from the University of Science and Technology of China, Hefei, China, in 2017. She is currently pursuing the M.Sc. degree in signal and information processing with the National Key Lab of Microwave Imaging Technology, Institute of Electronics, Beijing, China.

Her research interest includes machine learning in synthetic aperture radar imaging.

JIAN-PING LUO was born in Guizhou, China, in 1995. He received the B.Sc. degree in electronic information science and technology from Central South University, Changsha, China, in 2018. He is currently pursuing the Ph.D. degree in signal and information processing with the National Key Lab of Microwave Imaging Technology, Institute of Electronics, Chinese Academy of Sciences.

His research interest includes novel radar imaging techniques.

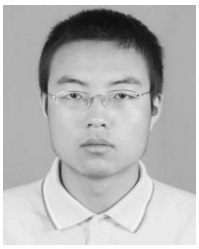

RUICHANG CHENG was born in Liaoning, China, in 1992. He received the B.Sc. degree in applied physics from the University of Science and Technology of China, Hefei, China, in 2015. He is currently pursuing the Ph.D. degree in signal and information processing with the National Key Lab of Microwave Imaging Technology, Institute of Electronics, Beijing, China.

His research interests include 3D reconstruction of objects from point clouds and deep learning in synthetic aperture radar imaging.

XING-DONG LIANG received the Ph.D. degree from the Beijing Institute of Technology, Beijing, China, in 2001.

Since 2002, he has been with the Institute of Electronics, Chinese Academy of Sciences, Beijing. During this period, he has product responsibility for many important Chinese national programs, including high-resolution synthetic aperture radar (SAR) systems, polarimetric and interferometric SAR systems, and preresearch for advanced SAR systems. He is currently a Professor with the National Key Lab of Microwave Imaging Technology, Institute of Electronics, Chinese Academy of Sciences. His research interests include real-time radar signal processing, coherent polarimetric and interferometric SAR systems, and novel radar imaging techniques.

Dr. Liang has been rewarded by the Chinese Government for his great contributions to the remote sensing area for several times.